JOURNAL OF SOLID STATE CHEMISTRY **133,** 273–278 (1997)
ARTICLE NO. SC977455

Impedance Spectroscopy and XPS Comparative Investigations of the State of Boron Atoms in an Amorphous Metallic Matrix

Iovka Dragieva, Zdravko Stoynov, and Iveta Nikolaeva

Central Laboratory of Electrochemical Power Sources, Bulgarian Academy of Sciences, 1113 Sofia, Bulgaria

and

Vesselin Krastev

Institute of General and Inorganic Chemistry, Bulgarian Academy of Sciences, 1113 Sofia, Bulgaria

Received April 14, 1997; accepted April 28, 1997

The purpose of this study is to compare the investigations of amorphous magnetic ribbons combining the usual structural methods with physical impedance spectroscopy (PIS) and X-ray photoelectron spectroscopy (XPS). The samples are commercially available rapidly quenched ribbons for torroidal transformers. Two types of ribbons were thermally treated below the temperature of amorphous–crystalline phase transition. Two binding energies of B 1*s* electrons are determined by XPS in one of the as-quenched ribbons, which show impedance time constant spectra without dispersion. The other ribbon, possessing only one value of binding energy of the B 1*s* electron (B^{I} state) in a rapidly as-quenched state, undergoes transition to a still amorphous state but acquires high electromagnetic losses and show another value of the binding energy of the B 1*s* electron (B^{II} state) after the heat-treatment procedure. This latter type of ribbons show structural impedance spectra containing various time constant values.

INTRODUCTION

The investigation of the magnetic impedance effect in amorphous alloys, ribbons, wires, and thin films, attracts growing attention. There are a number of scientific groups and researchers working actively in this field (1–10). The quality and quantity analysis data of the magnetic impedance effect in low coercive ferromagnetic and conductive materials, have been interpreted in terms of classic electrodynamics and classic magnetization processes.

Physical impedance spectroscopy (11) makes possible nondestructive control of the amorphous magnetic ribbons prior to the application of any type of thermal treatment or crystallization procedures with respect to their utility in the assembling of torroidal transformers.

The purpose of this study is to compare the investigations of the amorphous magnetic ribbons obtained by means of X-ray photoelectron spectroscopy (XPS) which is usually useful in studies of thin films, nanoparticles, (12, 13) and surface phenomena, with the data obtained by physical impedance spectroscopy (PIS).

EXPERIMENTAL

Table 1 presents some data on the contents of boron, hydrogen, and oxygen in the amorphous ribbons which are trademarked products of Asha Co., Russia (14).

Both types of ribbons, named A (86КАГСР, Asha Co.) and C(9КГР, Asha Co.) are 5 mm wide. They were heat treated for 1 h in vacuum furnace Heraeus, VT-5050, at 400°C with a vacuum of 5×10^{-3} Torr. The as-treated samples are denoted by A* and C* in the text. The temperature selected for the heat treatment procedure was far below the temperature of crystallization of both ribbons and they retain their amorphous state. There are no visible crystallization (X-ray diffraction, DTA (DSC) or TMA processes or enlargement of the metallic grains in both heat-treated ribbons A* and C* (11).

The heat effects of crystallization of ribbon type A (Table 1) decrease from 3.9 to 3.3 cal/g for ΔH_1 and from 8.05 to 6.49 cal/g for ΔH_2 of a type A* sample. The same influence of the annealing procedure on the partial crystallization process is evident for the samples of ribbon C (Table 1). The heat effect of crystallization of ribbon C is reduced from $\Delta H = 18.93$ cal/g to $\Delta H = 14.39$ cal/g for heat-treated ribbon C*.

The analysis of the light elements was carried out by titrimetric determination of boron and by vacuum extraction and gaseous analysis (with Balzers Exhalograph EA-1 and with Leco, RH-3) for the determination of hydrogen

0022-4596/97 $25.00

TABLE 1
Content of Light Elements in Amorphous as-Quenched Magnetic Ribbons

Parameters	Type of ribbons A (86 КГСР, Asha Co.)			Type of ribbons C (9KCP, Asha Co.)		
Width (mm)	5	10	20	5	10	20
Boron content (wt%)	2.70	1.30	3.46	3.76	4.07	3.28
Hydrogen content (wt%)	0.0313	0.0161	0.0064	0.0040	0.0095	0.0078
Oxygen content (wt%)	0.1240	0.0550	0.0230	0.0159	0.0289	0.0288
Heat effects (cal/g):						
Before ΔH_1, ΔH_2	3.9, 8.05	—	—	18.93	—	—
After annealing (*)	3.3*, 6.49*	—	—	14.39*	—	—

and oxygen. Other investigations related to the structural and magnetic properties were performed in (11, 14).

The impedance measurements were carried out at room temperature by a Solartron 1174 frequency response analyzer in the frequency range 999–100 kHz. To achieve high accuracy, the number of the integration periods was chosen to be 100 (11). In a PIS study the length of all samples should be chosen to be the same (in this case 150 mm) for all experimental measurements. The thickness of the ribbons was chosen to be the same (50 μm) and was negligibly small in comparison with the other two dimensions, length and width.

X-ray photoelectron spectroscopy (XPS) studies were carried out in an Escalab Mk II (VG Scientific) electron spectrometer (12). The photoelectron spectra were excited with a twin-anode X-ray source using Al$K\alpha$ excitation at 1486.6 eV. The instrumental resolution measured as the full width at half-maximum (FWHM) of the Ag $3d_{5/2}$ photoelectron peak was 1.3 eV and the C 1*s* photoelectron line at 284.6 eV was used as an energy reference level. To obtain the depth profiles of the elements, Ar^+ bombardment (etching time, 10 min) with beam energy of 3 keV and a current density of 5 $\mu A\,cm^{-2}$ was applied.

RESULTS AND DISCUSSION

Impedance Spectroscopy Study

The specimen impedance is very low, within in the range of few Ohms, where as in the inductive part the imaginary component dominates (15). Taking into account that the inductive component can also yield information on the microstructure of the metallic magnetic specimens (16), measurements were carried out in the 800 to 100 kHz frequency range, where the inductive part can be measured with sufficient precision.

Figure 1 presents the resistance (R) of the as-quenched specimens A (■) and C (□) and, after their heat-treatment procedure, treated specimens A* (●) and C* (○) measured as functions of frequency. It can be seen that after the heat-treatment procedure the resistance of samples A* and C* decreases within the whole frequency range.

Figure 2 presents the inductance (L) of specimens A (■) and C (□) before and after the heat-treatment procedure of specimens A* (●) and C* (○) as a function of frequency. As a result of the thermal treatment, the inductance of A decreases to the inductance of A* similarly to the previous case of resistance. In contrast, the inductance of ribbon type C* (○) is higher than that of the original as-quenched specimen type C^- (□).

Obviously, resistance and inductance as impedance components are more sensitive to small changes in the fine structure of the amorphous alloys caused by the applied heat treatment procedure than changes observed by the known structural methods, X-ray diffraction or DTA (DSC) and thermomagnetic analysis, which result in the amorphous state of all the specimens (11).

To indicate the possibilities for the application of the inductance in the impedance analysis of low resistive

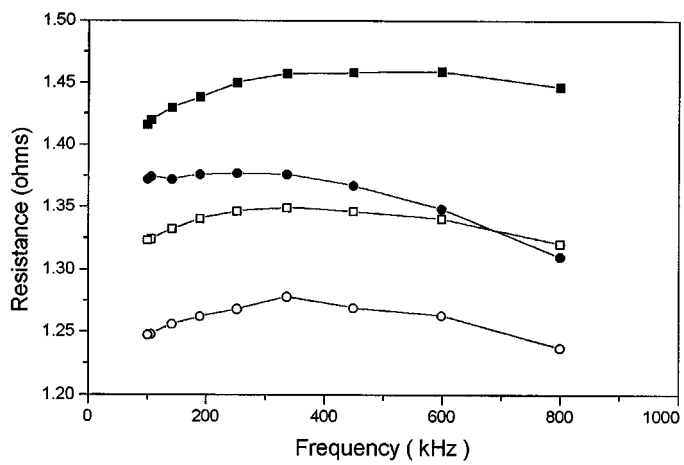

FIG. 1. Resistance (Ω) of sample A before (■) and of sample A* after annealing (●), and resistance of sample C before (□) and of sample C* after annealing (○), as a function of frequency.

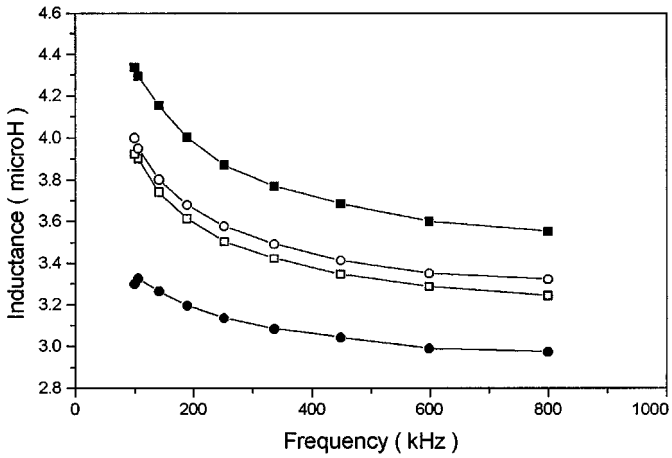

FIG. 2. Inductance (μH) of sample A, before (■) and of sample A* after annealing (●) and inductance of sample C before (□) and of sample C* after annealing (○), as function of frequency.

samples, all experimental results, measured on samples A (■), A* (●) and C (□), C* (○) are presented in Fig. 3. Here the intensive parameter vs frequency ($\log f$) is the ratio L/R possessing the dimension of a time constant or electromagnetic losses. After heat-treatment the electromagnetic losses of ribbon C are higher (ribbon C*).

The application of the structural approach (17) in the presentation of the impedance data results in very different time constant spectra of the two types of amorphous magnetic ribbons (11), which are very similar with regard to their magnetic and conductive properties, amorphous structures, and content of boron, but different with regard to the content of light atoms, hydrogen.

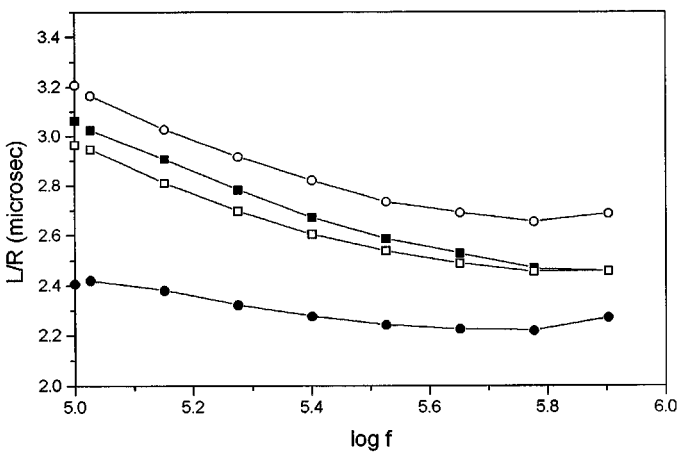

FIG. 3. Frequency dependence of the time constant L/R for the ribbons type A (■) and type C (□), before and after annealing: type A* (●), and type C* (○).

The general conclusion from the experimental data discussed above is that the inductive impedance component is very sensitive to the structural (or to the inductance and magnetic anisotropy) changes occurring in the investigated ribbons.

X-Ray Photoelectron Spectroscopy Study

Figure 4 presents XP spectra of 1*s* electrons of boron atoms in the type *A* ribbon. The initial spectrum (the untreated surface, Fig. 4, curve 1) is characterized by a low intensity peak of about 192 eV. The weak signal of the photoelectrons is due to the roughness of the surface. After 10 min of Ar^+ etching, two values of the binding energy (BE) (B^I and B^{II} states) of B 1*s* electrons are observed, 188.2 and 193.2 eV, respectively (Fig. 4, curve 2). The same two states of binding energy of B 1*s* electrons were observed in XPS investigation of amorphous nanoparticles obtained by means of a borohydride reduction process (12, 13) and they can be attributed to the different length of the chemical bonds in which the boron atoms participate (with hydrogen atoms too).

After a heat-treatment procedure occurs at 400°C, ribbon A* retains its X-ray amorphous state, and there is a very small decrease in both heat effects ΔH_1 and ΔH_2 belonging to the amorphous–crystalline transition (Table 1). It can be inferred from Fig. 4, curves 3 and 4, that a break has occurred in all the chemical bonds in which the boron atoms participate. According to the X-ray diffraction and DTA studies, there are neither any phase transitions nor

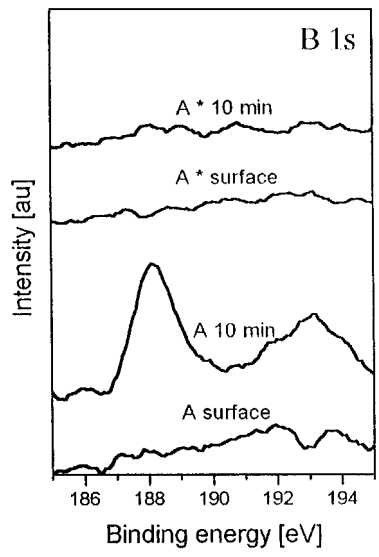

FIG. 4. XP spectra of B 1*s* electrons of as-quenched ribbon A, on the surface (curve 1), as-quenched ribbon A, after Ar^+ 10 min etching (curve 2), heat-treated ribbon A*, on the surface (curve 3), and heat-treated ribbon A*, after Ar^+ 10 min etching (curve 4).

crystallization processes during the heat treatment; however, some diffusion processes yielding bond breaking and mixing of the alloy constituents, especially the light atoms, such as boron and hydrogen, have occurred (Table 1, ribbon A). The mutual diffusion of boron and hydrogen produces boron depletion of the surface layer.

Figure 5 presents the XP spectra of 1*s* electrons of boron atoms in the type C ribbon. The initial spectrum (the untreated surface, Fig. 5, curve 1) is similar to that of Fig. 4, curve 1.

After 10 min of Ar^+ etching, one BE of B 1*s* electrons (B^I state) is observed (Fig. 5, curve 2). During the heat-treatment procedure, no phase transition or crystallization processes are detected, but the BE of B 1*s* electrons acquires another value (B^{II} state) on the surface of a heat-treated ribbon C* (Fig. 5, curve 3). The same B^{II} state is observed with a higher intensity after Ar^+ bombardment of the C* ribbon (Fig. 5, curve 4).

The X-ray photoelectron spectra from ribbons (A, A*) and (C, C*) of the Co 2*p* electrons are shown in Figs. 6 and 7, respectively. The heat treatment has little influence on the intensity of XP spectra of Co 2*p* electrons of ribbon A* (Fig. 6). In Fig. 7, curve 2, two peaks of BE are recorded, 777.6 and 783.6 eV. The first is due to metallic Co while the second results from Co–Fe bonding (for the composition of the ribbon C, see Table 1). The thermal treatment of ribbon C (Fig. 7) leads to the disappearance of the peak at 783.6 eV, suggesting bond breaking at the annealing temperature without occurrence of a phase transition.

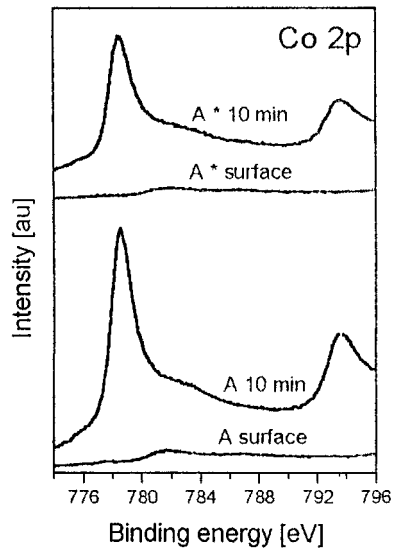

FIG. 6. XP spectra of Co 2*p* electrons of as-quenched ribbon A, on the surface (curve 1), as-quenched ribbon A, after Ar^+ 10 min etching (curve 2), heat-treated ribbon A*, on the surface (curve 3), and heat-treated ribbon A*, after Ar^+ 10 min etching (curve 4).

The X-ray photoelectron spectra taken from ribbons A, A* and C, C* of the O 1*s* electrons are shown in Figs. 8 and 9, respectively. Both figures show broad peaks, giving information about the existence of different oxygen containing compounds.

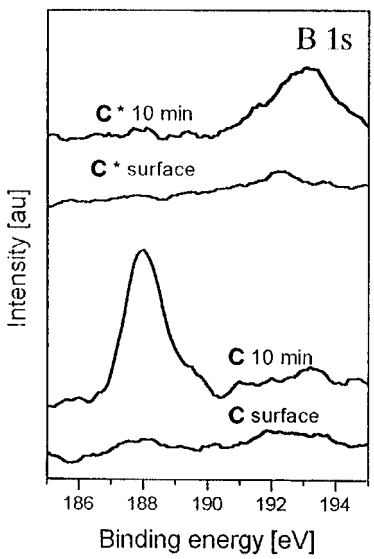

FIG. 5. XP spectra of B 1*s* electrons of as-quenched ribbon C, on the surface (curve 1), as-quenched ribbon C, after Ar^+ 10 min etching (curve 2), heat-treated ribbon C*, on the surface (curve 3), and heat-treated ribbon C*, after Ar^+ 10 min etching (curve 4).

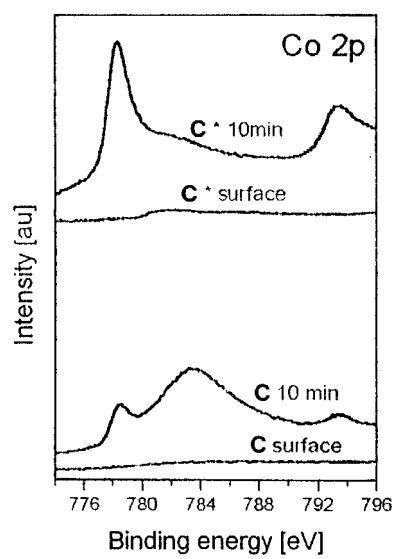

FIG. 7. XP spectra of Co 2*p* electrons of as-quenched ribbon C, on the surface (curve 1), as-quenched ribbon C, after Ar^+ 10 min etching (curve 2), heat-treated ribbon C*, on the surface (curve 3), and heat-treated ribbon C*, after Ar^+ 10 min etching (curve 4).

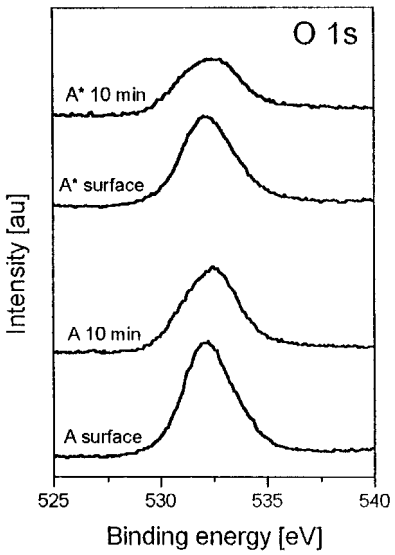

FIG. 8. XP spectra of O 1*s* electrons of, as-quenched ribbon A, on the surface (curve 1), as-quenched ribbon A, after Ar^+ 10 min etching (curve 2), heat-treated ribbon A*, on the surface (curve 3), and heat-treated ribbon A*, after Ar^+ 10 min etching (curve 4).

The heat treatment procedure performed in this study leads to the breaking of chemical bonds, initiation of a diffusion process, and growth of crystallization centers with the participation of the grain boundaries (or with the participation of boron and hydrogen atoms), resulting in a subsequently more stable, but still metastable, state according to XR diffraction traces and DTA(DSC) data (11).

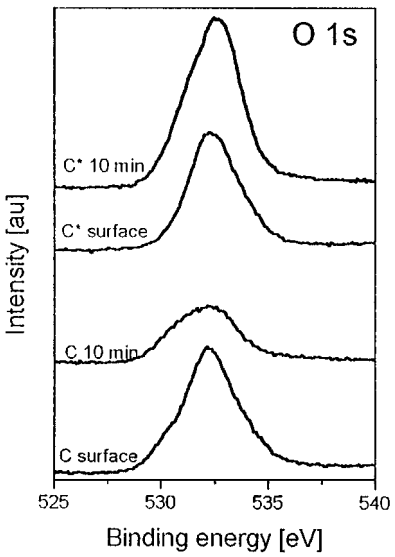

FIG. 9. XP spectra of O 1*s* electrons of as-quenched ribbon C, on the surface (curve 1), as-quenched ribbon C, after Ar^+ 10 min etching (curve 2), heat-treated ribbon C*, on the surface (curve 3), and heat-treated ribbon C*, after Ar^+ 10 min etching (curve 4).

CONCLUSION

The comparative investigations show that traditionally applied structural methods are not sensitive enough to the structural changes and properties of amorphous ribbons containing light elements, such as boron and hydrogen, which are often subjected to heat treatment at temperatures below those of the amorphous–crystalline phase transition for needs of practice.

Boron (and hydrogen) containing amorphous magnetic materials proved to be highly sensitive to the inductance (the imaginary part or magnetic anisotropy) of the impedance and its time constant spectra proved to be highly sensitive to the nanostructural changes incremented by the diffusion phenomena.

The presence of two binding energies of B 1*s* electrons to the boron nuclei is established irrespective of the shape, sizes, compositions, and methods of production of the amorphous materials. When the boron atoms are involved in amorphous magnetic substances, the two electrons belonging to the first quantum level (1*s*, $n = 1$) of the boron atom, the B 1*s*, vary in binding energy from 3.2 to 5 eV. This is proof that the azimuth quantum number (l) and magnetic quantum number (m_l) of these two B 1*s* electrons are not the same and are not equal to $l = m_l = (n - 1) = 0$, as should be expected in the case of a crystalline solid state.

ACKNOWLEDGMENTS

This work has been accomplished with the partial financial support of the National Science Fund, Ministry of Science and Education of Bulgaria, Project X-304.

REFERENCES

1. R. S. Beach and A. E. Berkowitz, *Appl. Phys. Lett.* **64,** 3652 (1994).
2. R. S. Beach and A. E. Berkowitz, *J. Appl. Phys.* **76,** 6209 (1994).
3. R. L. Sommer and C. L. Chien, *Appl. Phys. Lett.* **67,** 857 (1995).
4. R. L. Sommer and C. L. Chien, *Appl. Phys. Lett.* **67,** 3346 (1995).
5. K. V. Rao and F. B. Humphrey, and J. L. Costa-Kramer, *J. Appl. Phys.* **76,** 6204 (1994).
6. J. L. Costa-Kramer and K. V. Rao, *IEEE Trans. Magn.* **31,** 1261 (1995).
7. M. Knobel, M. L. Sanshez, C. Gomez-Polo, M. Vazquez, and A. Hernando, *J. Appl. Phys.* **79,** 1646 (1996).
8. K. Mohri, L. V. Panina, T. Uchiyama, and M. Noda, *IEEE Trans. Magn.* **31,** 1266 (1995).
9. L. V. Panina, K. Mohri, K. Bushida, and M. Noda, *J. Appl. Phys.* **76,** 6198 (1994).
10. K. Mohri, K. Bushida, M. Noda, H. Yoshida, L. V. Panina, and T. Uchiyama, *IEEE Trans. Magn.* **31,** 2455 (1995).
11. I. Dragieva, Z. Stoynov, E. Lefterova, and M. Mintchev, *Bulgarian Chem. Commun.* **27**(3–4), 570 (1994).

12. V. Krastev, M. Stoycheva, E. Lefterova, I. Dragieva, and Z. Stoynov, *J. Alloys Compounds* **240**(1–2), 186 (1996).
13. I. Dragieva, Z. Stoynov, V. Krastev, and P. Peshev, *J. Solid State Chem.* in press.
14. I. Dragieva, M. Mintchev, and M. Stanimirova, "Proc. INTER-MAG'93, Stockholm, Sweden, April 1993, FR-12."
15. B. Savova-Stoynov and Z. Stoynov, *J. Appl. Electrochem.* **17,** 1150 (1987).
16. Z. Stoynov, B. Savova-Stoynov, and T. Kossev, *J. Power Sources* **30**(1–4), 301 (1990).
17. Z. Stoynov, *Electrochim. Acta* **34,** 1187 (1989).